Unlocking the true power of additive manufacturing for EMI shielding

Markus G. Scheibel[1], Michael P. Kaiser[2], Sutharsan Balasubramaniam[2], Mykola Chernobryvko[2], Julia-Marie Köszegi[2], Marc Dreissigacker[2], Marius Adler[2], Tanja Braun[2], Chuan I "Eric" Huang[1], Meng "Jason" Li[1], Muriel Thomas[1], Franz Vollmann[1]

[1]Heraeus Electronics GmbH & Co.KG
Heraeusstr. 12-14
63450 Hanau, Germany
Ph: +49-6181-353682

[2] Fraunhofer-Institute for Reliability and Micro integration
Gustav-Meyer-Allee 25,
13355 Berlin, Germany
Ph: +49-30-46403207;

Email: markus.scheibel@heraeus.com

Abstract

Miniaturization trends in electronic packaging led to reduced spacing of individual packages on the printed circuit boards and thus increased the overall electromagnetic interference (EMI) levels within a device. State-of-the-art conformal coatings as EMI shielding layers are typically applied via sputter technology and offer design limitations with respect to coating selectivity on individual positions of the overall package. Our new technology of additively Ag layer application via inkjet printing overcomes today's design limitations and is key enabler for next generations packaging designs.

In this study, we compare the shielding effectiveness (S.E.) on specifically designed transmission line emitter samples coated with state-of-the-art sputtered conformal layers against silver coatings applied via inkjet printing of particle free metal organic decomposition inks to evaluate the new technology for its potential on package level shielding performance. Mechanical and electrical characterization of the silver coatings indicate appropriate tools to specify layer characteristics and ensure S.E. of 40 dB or higher at frequencies of 800 MHz and higher. The suitability of our well-tailored silver coatings to match typical S.E. requirements is shown with even much thinner layer thickness as compared to state-of-the-art coatings.

Key words

Printed Electronics, Inkjet Printing, EMI shielding, 5G, System in Package, Package-level shielding

I. Introduction

The miniaturization trends in PCB board design and advanced semiconductor packaging have been proceeding for decades. As a result, the spacing between the individual packages is decreasing drastically and thus the electromagnetic noise within the electronic device is increasing, accordingly [1]–[6]. In order to prevent a degradation in device performance or even failure, the initial approach of shielding enclosures was replaced successively by board level shielding and later package level shielding. The number of shielded devices is increasing just as much as the requirements for total shielding effectiveness (S.E.) [7], [8].

A typical example of a package which is strongly affected by electromagnetic interference (EMI) is a system in package (SiP). These kinds of subassemblies commonly consist of a glass fiber reinforced substrate (i.e., FR4) carrying the semiconductors and covered by a molding cap of an electromagnetically transparent epoxy molding compound (EMC). The EMC cap is typically overcoated with a

conformal coating that serves as the EMI shielding layer. The electrically conductive structure acts as a Faraday cage and inhibits the propagation of electromagnetic radiation in a range from several hundreds of MHz up to $\geq$ 6 GHz for 5G application. The shielding layer is grounded by a connection to the substrate's reference plane that enables the shielding functionality.

Beyond the application for EMI management, conductive coatings are exploited in the context of hardware security to prevent and/or detect physical attacks on ICs [9].

Today's shielding layers are typically conformal coatings applied using gas phase deposition technologies such as physical vapor deposition (PVD) or sputtering and build up layers of two alternating steel use stainless (SuS) layers and a center Cu layer in typical thicknesses of SuS/Cu/SuS of 2/4/2 µm or 0.18/3.8/0.18 µm, respectively.

New trends in electronic packaging raise the requirements for more selective coatings and go beyond current design limitations originating from unselective shielding layer application methods. The electronic systems of the next decade demand a new generation of shielding technology. Additive manufacturing is a prime candidate to meet these needs.

Additive manufacturing technologies such as inkjet printed electronics of silver inks gain increasing interest in selective application of functional coatings, such as conductive layers. Heraeus developed a turnkey solution for printing equipment, curing process and particle free metal-organic decomposition (MOD) silver ink materials that ensure long open time (~ 1 month) on the printer and provide a coating technology that can easily tailored to each individual package design by adjusting the digital printing profile in the printer software. Coating layer specifications for quality assurance of conformal EMI shielding layers are still limited to experienced values derived from sputter technology and are not accounting the performance potential of selective coating technologies.

Within this study, we extract the S.E. performance of selectively applied silver coatings by inkjet printing on specifically designed transmission line packages and compared against state-of-the-art sputtered samples. Mechanical and dielectric characterizations of silver coating layers will provide a fundament for characterization and specification of such layers as basis for quality assurance requirements. The respective sample layouts and testing characteristics will be described and a principal overview of basic S.E. theory will be given.

II. Shielding by inkjet printed Ag coating

A. EMI shielding

In general, there are three different mechanisms that contribute to EMI shielding. Each describes one interaction of electromagnetic waves at a material interface with different magnetic and dielectric properties:

1. Absorption $A\ (dB)$
2. Reflection $R\ (dB)$
3. Multireflection $M\ (dB)$

The electromagnetic wave can be absorbed by inducing currents in the conductive shielding materials that are removed via the grounding of the coating and result in an attenuation of the incoming wave longitudinal over the penetration depth (δ). The penetration depth

$$\delta = \sqrt{\frac{\rho}{\pi f_0 \mu_r \mu_0}} \tag{1}$$

depends on the absorbed wave frequency (f_0), the resistivity of the shielding layer (ρ), its relative permeability (μ_r) and the vacuum permeability (μ_0). The absorption is the dominant shielding mechanism at high frequencies. At low frequencies, the skin depth is increasing, and a comparatively high shielding layer thickness must be realized for sufficient attenuation via absorption.

Reflection, as the second shielding mechanism, occurs at the interface of two media with different wave propagating properties, namely a different intrinsic wave impedance η. The wave impedance is a function of magnetic permeability (μ) and dielectric permittivity (ε). A plane wave travelling in free space experiences the impedance of

$$\eta_0 = \sqrt{\frac{\mu_0}{\varepsilon_0}} = 377\ \Omega. \tag{2}$$

Within a non-conductor, the impedance η_{NC} is determined by the permeability and permittivity of the respective material

$$\eta_{NC} = \sqrt{\frac{\mu_0 \mu_r}{\varepsilon_0 \varepsilon_r}} \tag{3}$$

and for conductors, η_C is dependent on the frequency of the incoming wave and on the electrical conductivity of conducting materials in addition.

$$\eta_C = \sqrt{\frac{2\pi f \mu_r}{\sigma}}. \tag{4}$$

Finally, the fraction of the incoming wave that is neither initially reflected at the surface of the shielding nor dissipated within the shielding can be reflected multiple times at the interfaces of shielding material and e.g., air. As a result, the effectiveness of the shielding is decreased. This multireflection plays an important role particularly for low frequencies and thin shielding layer thicknesses (t) (5).

$$M = 20\ log\left|1 - e^{-2\frac{t}{\delta}}\right| \tag{5}$$

Hence, the total S.E. of a metal coating is composed of

$$S.E.(dB) = A\,(dB) + R\,(dB) + M\,(dB). \quad (6)$$

B. Measurement setup

For the characterization of the package-level S.E., a device under test (DUT) is developed consisting of a four-layer printed circuit board (PCB) which is covered with an EMC as can be seen in Figure 1. The EMC acts as a base for the application of the shielding material, i.e., sputter stacks of SuS/Cu/SuS with 0.18/3.80/0.18 and 2/4/2 µm layer thicknesses as the state-of-the-art reference to compare against silver in various thicknesses applied by inkjet printing. This methodology to assess the S.E. of metal coatings has successfully been used in previous studies [7], [10], [11].

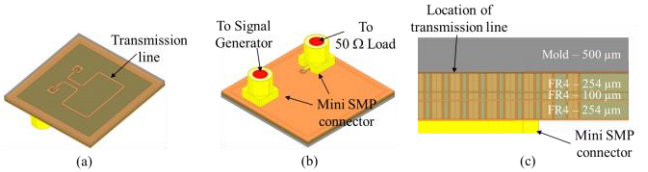

Figure 1: Overview of DUT. (a) Transmission line on top layer of PCB. (b) Bottom layer of PCB with Mini SMP connectors. (c) Stack-up of the DUT.

The DUT size is 20x20 mm^2. On the PCB's top layer, a 50 Ω transmission line is placed as a radiating source (Figure 1 (a)). This transmission line is connected by through hole vias to the bottom layer of the PCB, where two Mini SMP connectors are mounted (Figure 1 (b)). One connector is used to interface to an excitation source, whereas the second is terminated by 50 Ω. The two inner layers of the PCB are reference planes for the transmission line and the connector section, respectively. By applying ground vias, any resonances between the reference planes are suppressed. In addition, leaking fields at the PCB's edges can be prevented. To measure the S.E., the magnetic field radiated by shielded and unshielded DUTs are analyzed by applying a near-field scanning system as shown Figure . The setup consists of a DUT holder, a probe positioning system, where the magnetic field probe is located, and a signal generator as well as a spectrum analyzer which can create and capture RF signals at least up to 6 GHz. Due to the relation

$$S.E. = 20\,log\,\frac{H(\boldsymbol{r})}{H'(\boldsymbol{r})}, \quad (7)$$

where $H(\boldsymbol{r})$ and $H'(\boldsymbol{r})$ are the measured magnetic fields of the unshielded and shielded DUTs at a specific location $\boldsymbol{r}$, a quick estimation of the S.E. properties can be carried out. In the present study, the probe always stays at the center of the DUT when the S.E. is determined.

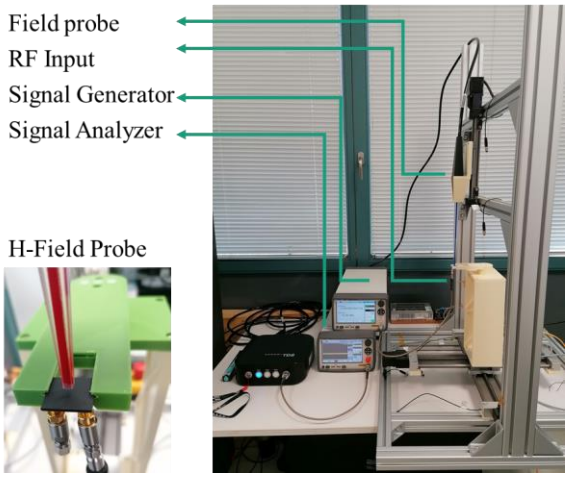

Figure 2: Near-field measurement setup for magnetic field S.E. evaluation.

Initial S.E. measurements on the sputtered reference samples with increasing distance between probe and sample surface (z-direction sweep) results in two opposite trends (Figure): For higher frequencies > 4.5 GHz, the S.E. decreases with increasing probe to surface distance, which is understood upon significant backside radiation originated from leakage at the SMP connectors on the sample backside (Figure (a)). Accordingly, x/y position sweeps indicate symmetrical S.E. drop towards the DUTs edge if the probe is moved symmetrically on x-direction with respect to the placement of the SMP connector on the sample backside (Figure (b)). If the probe is closer to the DUT edge adjacent to the SMP connectors monitored within a y-sweep (Figure (c)), an asymmetric drop in S.E. indicates a stronger interference coming from the radiation leakage at the respective connector. These measurements are performed at constant z-distance of 3 mm. Accordingly, proximity between probe and sample surface results in a shadowing, that reduces bias effects from backscattering radiation originated from the SMP connectors.

The S.E. however reaches a maximum at probe distance of 3 mm for low frequencies $\leq$ 4.5 GHz (Figure (a)), that has been described earlier as increasingly pronounced geometrical sensitivity based on mechanical artefacts with influences on the relative orientation between probe and sample surface changes in the angle of the incoming wave with respect to the probe surface [11]. Consequently, all S.E. values were extracted by a probe distance of 3 mm for f $\leq$ 4.5 GHz, to minimize artefacts of geometrical factors, and the biased back scattering at 6 GHz is corrected upon using the S.E. at a probe distance of 1 mm.

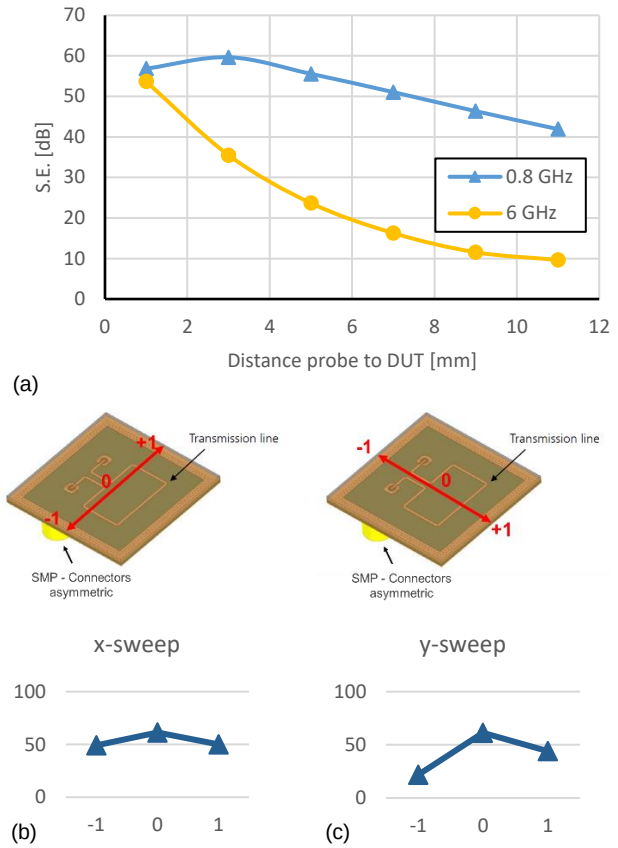

Figure 3: Overview of probe distance characteristics. (a) Dependency of S.E. on probe distance for two frequencies. (b) Symmetric x-sweep with respect to position of Mini-SMP connectors. (c) Asymmetric y-sweep with lower S.E. at position with close probe proximity to SMP connector.

C. Characterization of Ag coating layers

Within the Prexonics® System solution, a new technology for EMI shielding layer application is combining the advantageous particle free MOD silver ink and an Heraeus inkjet printer for EMI shielding using maskless selective coating. It offers a perfectly matched solution comprising application equipment, silver ink, and printing/curing processes to create the optimal conductive coating, providing design flexibility for varied pattern layouts. Non-selective material deposition methods such as plating, spray or sputter technologies achieve selective layer application only by masking/taping techniques. In contrast, precise application of silver layers on the desired position on the five sides of a package allows for well-tailored shielding layer designs. This enables inserting trenches, stand-off coatings or further surface features, such as laser markings and QR codes and encourages to inspire package designers to elaborate beyond today's design rules, simply by changing the digital printing picture.

The MOD ink technology itself is based on a fully dissolved silver precursor in a non-polar solvent system that ensures superior open times of several weeks on the printer (floor-live) and offers outstanding stability (shelf live) to enable transfer into mass manufacturing using uncritical chemistry without the requirements for special working environments (ATEX, etc.). The industrial scale inkjet printer is equipped with a specifically designed processor that translates the CAD coating drawing into accurate selectively coated components, which are processed in magazines of 300 mm ring carriers on which the components to coat are placed. All process steps are automated and inline: surface pre-treatment via atmospheric plasma process, inkjet printing of the MOD metal ink and sintering to a metallic coating film. Therefore, we designed an outstanding printing device to ensure stable printing conditions with technology leading printing accuracy ready for light-off factory manufacturing as single workstation equipment to be implemented into the full continuous wafer manufacturing process for semiconductor industry. The tool fulfills the standards of the semiconductor industry, and its mass production capability has been proven. The DUTs to investigate package level shielding performance were conformally coated using Heraeus Prexonics® MOD inks upon addition of an increased number of ink layers calculated for 208 nm silver per layer to build up a series of samples differing for their respective average layer thickness. The ink was cured using a UV curing profile of 120 s at a maximum temperature of 180 °C full inline to result in finalized silver coating layers showing an average conductivity of 17% $\sigma(Ag_{Bulk})$ (bulk silver conductivity) determined by 4-point probe measurements (s. Figure 4**Error! Reference source not found.**).

Figure 2: Dependency of electrical performance (sheet resistance (blue), contact resistance (red) and bulk of Ag conductivity (green)) on layers thickness.

At low coating thicknesses, an increase of relative conductivity with respect to $\sigma(Ag_{Bulk})$ indicates an incomplete sintering stage of the thin layers, that becomes constant at layer thicknesses of minimum 1.64 µm, which represents the thinnest layer for full interpretation within the course of this study. Thicker layers further exhibit the expected trend of decreasing sheet- and contact-resistance with the coating layer thickness. The contact resistance determined as electrical resistance between sample backside (grounding) and center position of the top of the coating reflects the sheet resistance trend from four-point probe

measurement and serves as a suitable characteristic to describe the electric performance of the sintered Ag coating. The layer thickness homogeneity was further characterized by X-ray fluorescence measurement based on the signal intensity from silver on EMC and externally referenced by a signal to thickness correlation derived by cross section and microscopy analysis.

The position dependent coating thickness over the sample surface (**Error! Reference source not found.**) does not i ndicate any accumulation of silver at certain remarkable positions (e.g., center), but indicates a random distribution over the whole sample surface.

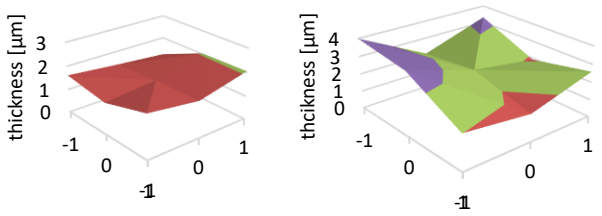

Figure 3: Position dependent Ag layer thickness mapping over the package surface by X-ray fluorescence analysis for a target layer thickness of 1.64 µm (left) and 2.67 µm (right).

A detailed distribution analysis (Table 1) shows that all samples thickness measurements on the top side match well with the target. However, the significantly high standard deviation over all nine positions within two individual samples indicate inhomogeneous layer distribution, which is further reflected by the large total deviation

$$Deviation = \frac{t_{max} - t_{min}}{2 * t_{average}} . \quad (8)$$

Table 1: Extracted average coating thickness compared with target thickness on sample top side.

	Unit	sample	
Target thickness	[µm]	1.640	2.670
Measured Average thickness on top side	[µm]	1.622	2.607
Standard deviation	[µm]	0.279	0.792
Deviation	[%]	25	47

A distinct layer thickness validation via microscopic studies on samples prepared from cross section allows rationalizing the unevenness of the surface thickness (Figure). The silver ink is initially following the conditions given from the substrate surface topology, and fluid properties will accordingly fill out the valleys on the top side, leaving a lower coverage on the summits of individual grain tips (Figure , center). Note that all filler particle indicated as spherical grey structures are covered by epoxy resin on the top side. However EMC-free grains are found at the sample sidewalls (Figure left). Accordingly, the side walls topology exhibits an even stronger expressed waviness as compared to the top side, and ink distribution is more driven by gap filling based forces on the inks surface tension at the sample side wall, then gravity as on the sample top side. If large grains are present on the sidewall surface, a low coating thickness is resulting at the most outer position of the resulting grain, and a larger thickness results vice versa at the position of pitch between grain and EMC.

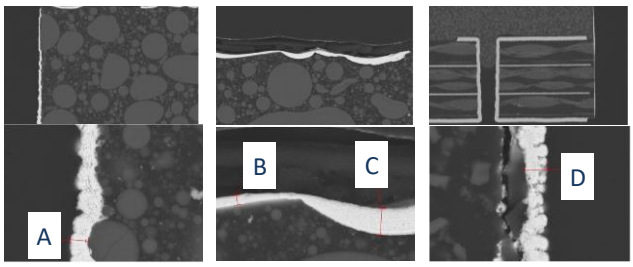

Figure 6: Microscopy analysis after sample preparation via cross section of sample with average thickness of 2.67 µm (at the sidewalls (left and right), and the top side (center)). Selective thickness measurements are given at representative spots A = 2.1 µm, B = 1.1 µm, C = 3.1 µm and D = 2.6 µm.

The overall surface coating thickness is highly depending on the individual measured spot and therefore only average values give a reliable indication on the coating layer quality from inkjet printing and is well in line with the observed match in average thickness. Accordingly, average values such as thickness over the full substrate surface, or electrical conductivity are much better suited measures to describe the coating layers characteristics.

Comparison of the average layer thickness on top side to side wall results in an average aspect ratio of 1.27 for 1.64 µm coating thickness and 1.36 for 2.67 µm, respectively. Sample preparation for this study was focusing on conformal package coating and did not emphasis the importance of a distinct top side to sidewall aspect ratio. However, digital inkjet printing allows for individual treatment of each package layer even in the conditions of mass manufacturing equipment, and the results clearly indicate no limitations on certain maximum coating ratios, but full design freedom.

D. Characterization of Ag coating S.E.

The S.E. trend of Ag coated transmission line packages indicate a linear dependency on the frequency (logarithmic, Figure). There is a significant difference between both investigated coating layer thicknesses of 2.67 µm and 1.64 µm, that is particularly observable at low frequencies. At higher frequency $\geq$ 2.4 GHz, all shielding values are well above medium shielding levels of 40 dB and differences in total shielding are within the error of the sample campaign.

An interpolated line indicates predictable shielding trends that allow for interpolation within the measured frequency range. There is an unexpected low shielding performance

found for all samples at 1 GHz, that indicates weaker shielding than at even lower frequency of 800 MHz, which contrasts with common shielding theory. However, shielding values at both low-end frequencies are within the error deviation and no systematic trend is assumed.

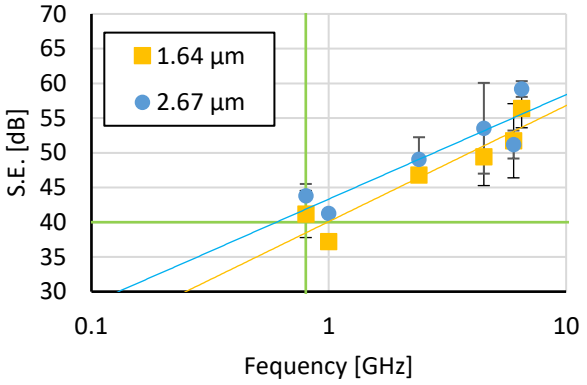

Figure 7: Magnetic S.E. of Ag coated samples with an average layer thickness of 1.64 µm (yellow) and 2.67 µm (blue) as a funciton of the incomming wave frequency and measured at a distance of 3 mm ($f \leq 4.5$ GHz) and 1 mm ($f > 4.5$ GHz) resepectively. The green lines mark typical stepcifications of S.E. = 40 dB at f_{min} = 800 MHz.

Typical shielding requirements define an overall S.E. at minimum frequencies of 800 MHz to at least 40 dB, as indicated by the green lines (Figure).
Commonly, S.E. is evaluated as a function of layer thickness. The data in Section II.C indicates that the inkjet printed layers exhibit an increased variation in thickness which does not affect the shielding capabilities. Hence, alternatively, the S.E. can be correlated with the respective contact resistance as a more reliable average characteristic of the silver coating (Figure).

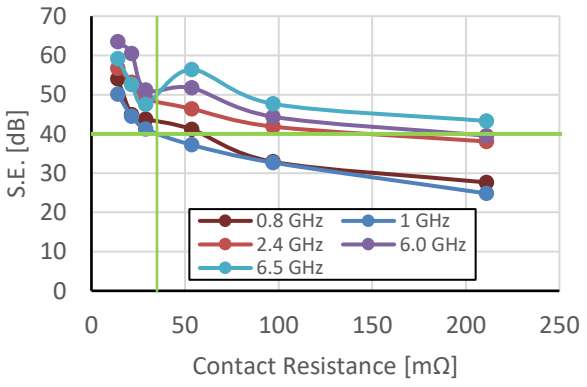

Figure 8: Dependency of S.E. on the contact resistance of the coating layers and typical specifications at 40 dB and 800 MHz (green lines).

Accordingly, ideal average coating thickness to achieve these requirements are between 1.64 and 2.67 µm and contact resistance specifications indicate an ideal performance for the respective package design of 35 mΩ.

E. Comparison to Cu state-of-the-art

Finally, the DUT of the present study was applied to the standard EMI shielding coating with standard sputter application parameters and addressed for layer thicknesses of SuS/Cu/SuS 0.18/3.80/0.18 µm and 2/4/2 µm. Figure 9 displays the results of the S.E. evaluation. The mean S.E. measures identically for both surface stack variants within the standard deviation of both samples with max/min values of 60 dB at 800 MHz and 49 dB at 2.4 GHz. The total S.E. does not indicate a dependency on the respective frequency. The difference in shielding performance for the two coating variants is minor and only observable for the low frequency range.

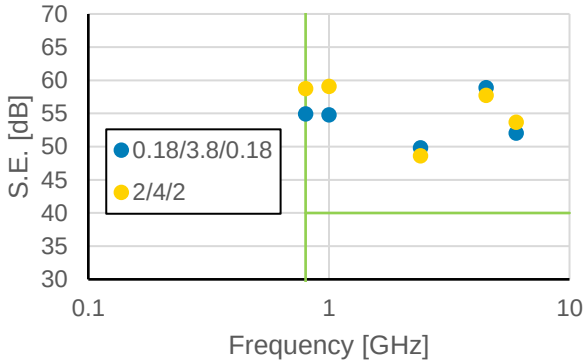

Figure 9: S.E. of sputtered samples with layer stacks of SuS/Cu/SuS in two stack thickness variants over the frequency.

From the application point of view, there is no significant difference in the shielding performance between silver coatings (selectively applied via inkjet printing of particle free MOD silver inks), and conformal coatings of three layer stacks via sputtering technology at frequencies of $\geq$ 2.4GHz. A tradeoff in shielding performance is only observable for low frequency magnetic shielding, however, sputtering is exceeding typical requirements by factors and thus indicates an oversizing of the package coating with potential to save in time and material/energy for shielding layer production.

III. Conclusion

In summary, EMI shielding properties of thin silver layers applied by selective inkjet printing from particle free MOD inks have been determined on specifically designed transmission line packages and compared against state-of-the-art shielding layer stacks of SuS/Cu/SuS 2/4/2 µm and 0.18/3.80/0.18 µm. The results indicate a frequency independent S.E. between 49 and 60 dB for all coating variants and indicate a minimal required coating thickness between 1.64 and 2.64 µm for Ag to achieve S.E. of $\geq$ 40 dB at frequencies of $\geq$ 800 MHz. While the coating displays distinct variation in thickness, this does not degrade the S.E. by any means.

In comparison, the state-of-the-art sputter coating technology exhibits a significant overachievement of typical S.E. specifications, which indicates a significant overcoating of the sample top-side. The respective electrical properties, i.e., contact resistance of standard sputter coatings represent the oversized performance, and thus do not serve as appropriate measure to benchmark well-tailored shielding layers. In contrast, correlations on S.E. on contact resistance must be drawn for new packages, to ensure full usage of design freedom benefits.

Selective silver deposition via additively inkjet printing of particle free MOD silver inks allows for breaking current design rules and establishing conformal coatings with adjustable aspect ratios of 1:1 or higher.

Typical quality inspection items like coating layers electrical conductivity derived from sputtered references with overcoated top side dimensioning are not suited to unleash the full performance and economical potential of new technologies. Redefinition of specification items to ensure mass production quality requires extraction of the true needs of a well-tailored shielding layer.

References

[1] R. Tummala, *System on package: miniaturization of the entire system.* McGraw-Hill Education, 2008.

[2] D. Manessis, L. Boettcher, S. Karaszkiewicz, A. Ostmann, R. Aschenbrenner, and KD. Lang, “Chip embedding technology developments leading to the emergence of miniaturized system-in-packages,” *IEEE 18th European Microelectronics & Packaging Conference*, 2011.

[3] K. Hollstein, and K. Weide-Zaage, "Advances in packaging for emerging technologies," *IEEE Pan Pacific Microelectronics Symposium*, 2020.

[4] C.A. Riso, et al. "Advanced Packaging Roadmaps and Government Needs," in *Proc. Government Microcircuit Applications and Critical Technology (GOMACTech)*, Miami, 2022, pp. 21–24.

[5] T. Löher, D. Schütze, M. Spanier, A. Ostmann, and M. Schneider-Ramelow, "PCB Embedding Technology for the Miniaturization of complex electronic systems," *2022 IEEE CPMT Symposium Japan (ICSJ)*, 2022.

[6] N. Kim, L.H. Li, S. Karikalan, R. Sharifi, and H. Kim, "Package-level electromagnetic interference analysis," *IEEE 64th Electronic Components and Technology Conference*, Orlando, 2014.

[7] J. Hoang, R. Darveaux, T. LoBianco, Y. Liu, and W. Nguyen, "Breakthrough packaging level shielding techniques and EMI effectiveness modeling and characterization," *IEEE 66th Electronic Components and Technology Conference*, Las Vegas, 2016, pp. 1290–1296.

[8] B. Kim, H. Jeon, D. Park, G. Kim, N. Cho, and J. Khim, "EMI shielding leadless package solution for automotive," *Journal of Advanced Joining Processes*, vol. 5, 2022, p. 100102.

[9] M. Nagata, T. Miki, and N. Miura, "Physical attack protection techniques for IC chip level hardware security," IEEE Transactions on Very Large Scale Integration (VLSI) Systems, vol. 30, 2021, pp. 5–14.

[10] N. Karim, J. Mao, and J. Fan. "Improving electromagnetic compatibility performance of packages and SiP modules using a conformal shielding solution," *IEEE 2010 Asia-Pacific International Symposium on Electromagnetic Compatibility*, Beijing, 2010, pp. 56–59.

[11] L. Ding, et al. "Near-field scanning based shielding effectiveness analysis of system in package," IEEE Transactions on Components, Packaging and Manufacturing Technology, vol. 11, 2021, pp. 1235–1242.